[68]Ga-Labeled Prostate-Specific Membrane Antigen Is a Novel PET/CT Tracer for Imaging of Hepatocellular Carcinoma: A Prospective Pilot Study

Mikhail Kesler[1], Charles Levine[1], Dov Hershkovitz[2,3], Eyal Mishani[4], Yoram Menachem[5], Hedva Lerman[1,3], Yaniv Zohar[6], Oren Shibolet*[3,5], and Einat Even-Sapir*[1,3]

[1]Department of Nuclear Medicine, Tel Aviv Sourasky Medical Center, Tel Aviv, Israel; [2]Department of Pathology, Tel Aviv Sourasky Medical Center, Tel Aviv, Israel; [3]Sackler School of Medicine, Tel Aviv University, Tel Aviv, Israel; [4]Cyclotron Unit, Hadassah Hebrew University Hospital, Jerusalem, Israel; [5]Department of Gastroenterology, Tel Aviv Sourasky Medical Center, Tel Aviv, Israel; and [6]Department of Pathology, Rambam Medical Center, Haifa, Israel

[68]Ga-labeled prostate-specific membrane antigen (PSMA), a PET tracer that was recently introduced for the imaging of prostate cancer, may accumulate in other solid tumors, including hepatocellular carcinoma (HCC). The aim of this study was to assess the potential role of ^{68}Ga-PSMA PET/CT in the imaging of HCC. **Methods:** Included in this prospective pilot study were 7 patients who had HCC with 41 liver lesions: 37 suspected malignant lesions (tumor lesions) and 4 regenerative nodules. For each liver lesion, the uptake of ^{68}Ga-PSMA and the uptake of ^{18}F-FDG were measured (as SUV and lesion-to-liver background ratios [TBR-SUV]) and correlated with dynamic characteristics (Hounsfield units [HU] and TBR [TBR-HU]) obtained from contrast-enhanced CT data. Immunohistochemical staining of PSMA in the tumor tissue was analyzed in samples obtained from 5 patients with HCC and compared with that of control samples obtained from 3 patients with prostate cancer. **Results:** Thirty-six of the 37 tumor lesions and none of the regenerative nodules showed increased ^{68}Ga-PSMA uptake, and only 10 lesions were ^{18}F-FDG–avid. On the basis of contrast enhancement, tumor lesions were categorized as 27 homogeneously enhancing lesions, 9 lesions with "mosaic" enhancement (composed of enhancing and nonenhancing regions in the same lesion), and a single nonenhancing lesion (the only non–[68]Ga-PSMA–avid lesion). The Mann–Whitney test revealed that ^{68}Ga-PSMA uptake was significantly higher in enhancing tumor areas than in nonenhancing areas and, in contrast, that ^{18}F-FDG uptake was higher in nonenhancing areas ($P < 0.001$ for both). ^{68}Ga-PSMA uptake (TBR-SUV$_{max}$) was found to correlate with vascularity (TBR-HU) (Spearman r, 0.866; $P < 0.001$). Immunohistochemistry showed intense intratumoral microvessel staining for PSMA in HCC; in contrast, cytoplasmic and membranous staining, mainly in the luminal border, was seen in prostate cancer samples. In 2 of the study patients, ^{68}Ga-PSMA PET/CT identified unexpected extrahepatic metastases. The 4 regenerative liver nodules showed no increased uptake of either PET tracer. **Conclusion:** ^{68}Ga-PSMA PET/CT was superior to ^{18}F-FDG PET/CT for imaging patients with HCC. HCC lesions are more commonly hypervascular, taking up ^{68}Ga-PSMA in tumoral microvessels. ^{68}Ga-PSMA PET/CT is a potential novel modality for imaging patients with HCC.

Hepatocellular carcinoma (HCC) accounts for about 80% of all primary liver cancer. It is the fifth most common cancer worldwide and the third most common cause of cancer-related mortality (*1*). Cirrhosis due to viral hepatitis and nonalcoholic fatty liver disease are leading risk factors for HCC (*2*). The disease is confined initially to the liver; however, the incidence of remote metastases from HCC has been reported to reach as high as 30% (*3*).

Current guidelines of the American Association for the Study of Liver Disease and the European Association for the Study of the Liver recommend HCC surveillance with abdominal ultrasound every 6 mo in patients at high risk of developing the disease. Patients diagnosed in early stages of HCC are eligible for potentially curative therapy. Therefore, early diagnosis and accurate staging are critical
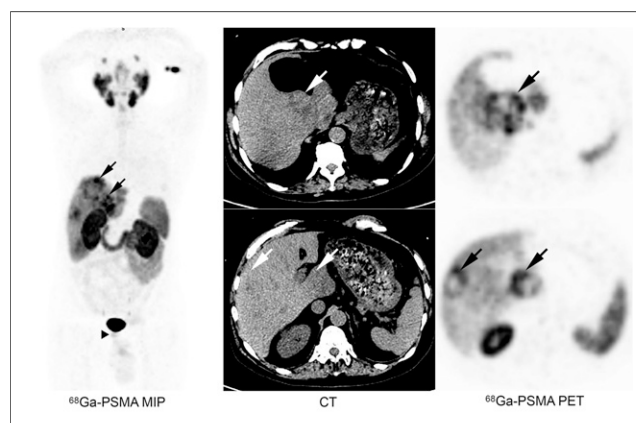
FIGURE 1. Incidental ^{68}Ga-PSMA–avid liver lesions detected in patient referred for ^{68}Ga-PSMA PET/CT because of newly diagnosed high-risk prostate cancer. Uptake of ^{68}Ga-PSMA was seen in prostate cancer (arrowhead) and liver lesions (arrows). After PET/CT, unknown HCC was diagnosed. MIP = maximum-intensity projection.

TABLE 1
Characteristics of Patients

Patient	Age (y)	Sex	Stage of disease	Predisposing risk for HCC	Chronic liver disease	Ch-P	PS	HTS*	AFP (ng/mL)
1	51	M	After TACE	HCV	Cirrhosis	B	1	T3	8
2	56	F	Initial staging	HBV	Cirrhosis	B	2	T3	46.6
3	62	F	Initial staging	HCV	Normal liver	A	0	T2	3,648
4	59	M	Initial staging	HBV	Cirrhosis	B	1	T3	5,336
5	38	M	Initial staging	HCV	Cirrhosis	B	1	T3	1,800
6	69	M	Initial staging	HCV	Fatty liver	A	1	T2	11
7	54	M	Initial staging	Familial HCC	Fatty liver	A	1	T3	4,000

*HTS = hepatic tumor stage based on morphologic imaging. Liver tumor stages: T2 = solitary tumor with vascular invasion or multiple tumors (<5 cm); T3 = multiple tumors of any size involving major branch of portal vein or hepatic vein.

Ch-P = Child-Pugh score (A = least severe liver disease; B = moderately severe liver disease); PS = Eastern Cooperative Oncology Group performance status (1 = restricted in physically strenuous activity but ambulatory and able to carry out work of a light or sedentary nature; 2 = ambulatory and capable of all self-care but unable to carry out any work activities; 3 = capable of only limited self-care; confined to bed or chair more than 50% of waking hours); AFP = α-fetoprotein; TACE = transarterial chemoembolization; HCV = hepatitis C virus; HBV = hepatitis B virus.

for a favorable prognosis. Curative-intent therapies for HCC include surgical resection, liver transplantation and, for small tumors, radiofrequency ablation (4).

Imaging of HCC at diagnosis is challenging, and assessment of HCC recurrence after treatment is even more difficult because it can be confounded by coagulative necrosis, hematomas, abscesses, and fluid or bile collections (5).

PET using ^{18}F-FDG has a limited role in evaluating patients with HCC because this tumor type is ^{18}F-FDG–avid in fewer than half of cases (6). ^{68}Ga-labeled prostate-specific membrane antigen (PSMA) is a PET tracer that was recently introduced for the imaging of patients with high-risk prostate cancer at diagnosis and patients with biochemical failure after treatment (7). Several case reports have described incidental increased uptake of ^{68}Ga-PSMA in other solid tumors (8). We recently performed ^{68}Ga-PSMA PET/CT in a patient with prostate cancer and noted increased uptake of the tracer at the primary prostate cancer site as well as additional "hot" liver lesions (Fig. 1). The latter lesions were confirmed to be HCC by biopsy.

That case prompted us to conduct a prospective pilot study to explore the potential role of ^{68}Ga-PSMA PET/CT in evaluating patients with HCC. ^{68}Ga-PSMA and ^{18}F-FDG PET/CT studies were performed in patients with HCC, and the results were compared with hemodynamic criteria derived from contrast-enhanced CT (ceCT) and MRI. We also assessed the immunohistochemistry of PSMA expression in biopsy samples obtained from patients with HCC and patients with prostate cancer as controls.

MATERIALS AND METHODS

Patient Characteristics

PET/CT studies were performed in 7 patients (5 men and 2 women) who were 39–68 y old and had HCC. The study was approved by the Institutional Review Board (The Tel Aviv Sourasky Medical Center Institutional Review Board [Helsinki Committee]), and patients signed a written informed consent form. Six patients were newly diagnosed, and 1 patient previously had undergone transarterial chemoembolization of the right liver lobe. None of

TABLE 2
PET Tracer Uptake and Contrast Enhancement of HCC Liver Lesions on CT and MRI

Patient	^{68}Ga-PSMA+ ^{18}F-FDG− Uptake	Enhancement Hom	Enhancement Mos	^{68}Ga-PSMA+ ^{18}F-FDG+ Uptake	Enhancement Hom	Enhancement Mos	^{68}Ga-PSMA− ^{18}F-FDG+ Uptake	Enhancement Hom	Enhancement Mos
1	6	6	0						
2	2	2	0						
3	1	1	0						
4	3	3	0	3	0	3			
5	2	2	0	1	0	1			
6	1	1	0				1	0	0
7	13	12	1	4	0	4			

Hom = homogeneous; Mos = mosaic.
Data are reported as number of lesions.
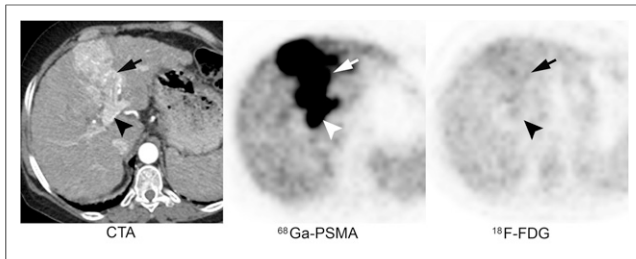
FIGURE 2. Enhancing HCC. Increased uptake of ^{68}Ga-PSMA was seen in tumor at left liver lobe (arrows) as well as in tumor thrombus in left portal vein (arrowheads). These lesions showed no ^{18}F-FDG avidity. CTA = CT angiography.

the patients had known extrahepatic spread before PET/CT. The characteristics of the patients are summarized in Table 1.

PET/CT Scan

All patients underwent 2 PET/CT scans, ^{68}Ga-PSMA PET/ceCT and ^{18}F-FDG PET/CT, 1–5 d apart using a Discovery 690 scanner (GE Healthcare). We used ^{68}Ga-PSMA with the precursor PSMA-11 (Good Manufacturing Practices quality; ABX). Administered doses were 148 MBq of ^{68}Ga-PSMA and 444 MBq of ^{18}F-FDG. CT acquisition was performed at 100, 120, or 140 keV, depending on the patient's habitus. PET reconstruction included time of flight; 3 iterations; 18 subsets with the filter cutoff set at 6.4; a standard z-axis filter; a matrix size of 256; and Q Clear (GE Healthcare) image reconstruction.

Correlation of PET Findings and Contrast Enhancement on CT and MRI

PET/CT data were interpreted by a single experienced expert. Liver sites showing uptake higher than liver background activity were considered abnormal lesions. Both the SUV of the liver parenchyma (background) and the SUV of hepatic lesions were measured using similar regions of interest. Target-to-background ratios (TBR) were calculated.

For all patients, ceCT was available for correlation (the CT part of PET/CT as well as separately done CT). For 3 patients, MRI was also available for correlation. All images were reviewed by a radiologist experienced in CT and body MRI. Hounsfield units (HU) measured in the lesions and in the background parenchyma on ceCT were recorded, and TBR-HU (tumor-to-background ratio of Hounsfield units) was calculated. Liver lesions identified on ceCT and MRI were categorized as being suggestive of malignancy (tumor lesions) if they showed contrast enhancement and early portal washout, if they took up either tracer, and if they grew compared with the findings on previous scans. Lesions were further defined as hypervascular or hypovascular. Hypervascular lesions were those showing prominent enhancement
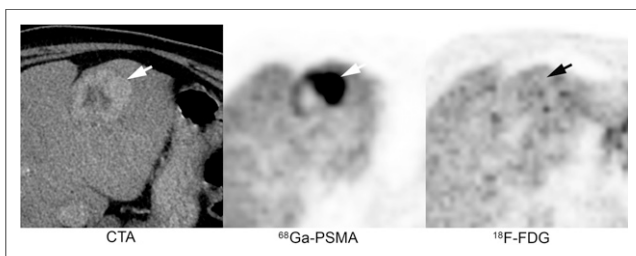
in the hepatic arterial dominant phase. Hypovascular lesions were those showing minimal enhancement in the hepatic arterial dominant phase and hypointensity compared with the liver background in delayed phases. Hypervascular lesions were subcategorized as being homogeneous or heterogeneous ("mosaic" pattern, in which enhancing and nonenhancing regions were found in the same lesion). On the basis of contrast enhancement, tumor areas were subcategorized as enhancing or nonenhancing.

Extrahepatic lesions found on PET/CT were also noted.

Immunohistochemistry of PSMA Expression in HCC and in Prostate Cancer Samples

A biopsy sample from liver tumor sites was available for the assessment of PSMA expression in 5 patients with HCC—3 patients from our cohort and 2 additional HCC patients who did not undergo PET/CT but for whom a CT study was available. For comparative purposes, samples from 3 patients with prostate cancer were also analyzed. One 4-mm slide was used for immunohistochemical staining. A slide of prostatic adenocarcinoma was used as an internal control. Immunostaining was performed using a monoclonal anti-PSMA antibody (NCL-L-PSMA; Novocastra) at a 1:80 dilution on an automated Ventana BenchMark XT Slide Stainer (Ventana Medical Systems).

PSMA expression was evaluated by 2 experienced pathologists. Any reactivity in either tumor cells or neoplastic vessels was considered to indicate a positive result. In the case of heterogeneous staining, the predominant pattern was recorded.

Statistical Analysis

SPSS software (IBM SPSS Statistics for Windows, version 25; IBM Corp.) was used for all statistical analyses. Variables were evaluated for normal distribution using histograms, and values were recorded as medians and interquartile ranges. These variables included HU and TBR-HU in the lesion on ceCT and SUV$_{min}$, SUV$_{max}$, and TBR-SUV (tumor-to-background ratio of SUV) for both ^{68}Ga-PSMA and ^{18}F-FDG on PET. The uptake values for the tracers in enhancing and nonenhancing lesions were compared using the Mann–Whitney test. The correlation between CT contrast enhancement and PET tracer uptake was obtained using the Spearman correlation coefficient. After linear regression was tested to meet expectations, it was used to illustrate graphically the correlation between ^{68}Ga-PSMA uptake (TBR-SUV$_{max}$) and vascularity (TBR-HU).

All statistical tests were 2-sided. A P value of less than 0.05 was considered statistically significant.

RESULTS

Imaging

Forty-one abnormal liver lesions, including 37 lesions considered to be tumor lesions on the basis of the prespecified criteria

FIGURE 3. HCC lesion with "mosaic" contrast enhancement. Increased ^{68}Ga-PSMA uptake was identified only in enhancing area (arrows). This HCC was non–^{18}F-FDG–avid. CTA = CT angiography.
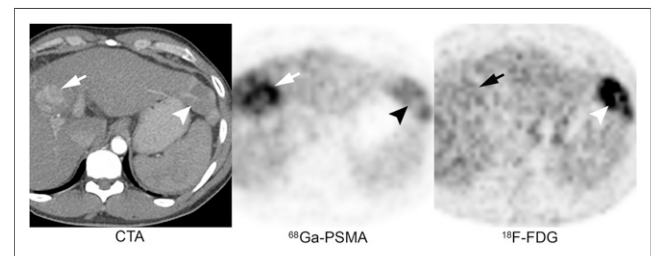
FIGURE 4. Coexisting HCC lesions revealed by ^{68}Ga-PSMA (arrows) and ^{18}F-FDG (arrowheads). Increased ^{68}Ga-PSMA uptake was seen in enhancing tumor lesion. CTA = CT angiography.

TABLE 3
Contrast Enhancement and ^{68}Ga-PSMA and ^{18}F-FDG Uptake in Homogeneous HCC Lesions and
in Areas Within Mosaic HCC Lesions

				CT				^{68}Ga-PSMA				^{18}F-FDG		
				HU		SUV		TBR-SUV		SUV		TBR-SUV	
Patient	Lesion	Area(s) within lesion	E or N	Lesion	TBR	Min	Max	Min	Max	Min	Max	Min	Max
1	1	1	E	114	2	9	11.7	3.1	3.2	1.4	1.8	1	0.9
	2	1	E	124.5	2.1	9.5	14.6	3.3	3.9	1.6	2.5	1.1	1.3
	3	1	E	128	2.2	5	8.2	1.7	2.2	1.6	2.1	1.1	1
	4	1	E	94.5	1.6	4.2	5.4	1.5	1.6	1.4	2.4	1	1.2
	5	1	E	89.7	1.5	7.8	9.5	2.7	2.6	1.6	2	1.1	1
	6	1	E	86.7	1.5	4.6	7.4	1.6	2	1.6	2.3	1.1	1.2
2	1	1	E	188.5	3.3	21	30.7	6.4	7.5	2.7	4.1	1.6	1.6
	2	1	E	144.5	2.4	6	11.1	1.8	2.7	2	3.1	1.2	1.2
3	1	1	E	99	1.6	10.5	17.5	3.3	3.6	3.8	6.5	2.5	3
4	1	1	E	117	1.3	9.1	13	3.4	3	1.8	2.8	1.1	1.2
	2	1	E	112	1.2	7.6	9.2	2.8	2.1	2.4	3.5	1.5	1.5
		2	N	84	0.9	2.9	6.4	1.1	1.5	6.4	9.4	4	3.9
	3	1	E	110.8	1.2	3.7	6.7	1.4	1.5	1.2	2.5	0.8	1
	4	1	E	77	0.9	4	6.6	1.5	1.5	2.8	3.2	1.8	1.3
		2	N	62	0.7	3.5	4.2	1.3	0.9	3.4	4.5	2.1	1.9
	5	1	E	110	1.2	9.2	14.7	3.4	3.3	1.9	2.5	1.2	1
		2	E	127.9	1.4	7.2	10.9	2.7	2.5	2	3	1.3	1.3
		3	N	71	0.8	2.6	3.9	1	0.9	2.7	2.9	1.7	1.2
	6	1	E	127	1.4	5.7	9.1	2.1	2.1	1.9	2.7	0.6	1.1
5	1	1	E	96.4	1.6	4.7	6.1	2.6	2.3	1.6	4.5	1.2	1.6
	2	1	E	109.8	1.8	7	9.6	3.9	3.5	1.7	2.7	1.3	0.9
	3	1	N	43.5	0.7	3.2	4.7	1.8	1.7	5.2	5.7	4	2
6	1	1	E	140	1.6	25.6	41.2	3.4	4.4	1.8	2.7	1	0.9
	2	1	N	62	0.5	3.7	8.3	0.5	0.9	5	7.3	2.9	2.4
7	1	1	E	75	1.9	11.4	11.9	4.2	3.7	2.4	3.8	1.3	1.4
		2	N	32.2	0.8	3.6	3.7	1.3	1.2	8.3	9	4.6	3.3
	2	1	E	69.8	1.8	9.4	14.8	3.5	4.6	2.6	2.9	1.4	1.1
	3	1	E	89.6	2.3	11.3	13	4.2	4.1	2.5	3.2	1.4	1.2
	4	1	E	94	2.4	13.6	17.3	5	5.4	2.4	2.7	1.3	1
	5	1	E	73	1.9	12.7	15	4.7	4.7	2.6	3	1.4	1.1
	6	1	E	92	2.4	12.5	16.3	4.6	5.1	2.5	3.3	1.4	1.2
		2	N	36	0.9	3.2	7.2	1.2	2.3	3.1	3.9	1.7	1.4
	7	1	E	76	1.9	10.2	12	3.8	3.8	2	3.7	1.1	1.4
	8	1	E	91	2.3	9.5	13.5	3.5	4.2	1.8	2.7	1	1
	9	1	E	115	2.9	10	14.3	3.7	4.5	2.3	3.2	1.3	1.2
		2	N	46	1.2	4.3	6.8	1.6	2.1	4	7.1	2.2	2.6
	10	1	E	97	2.5	12	13.3	4.4	4.2	2.1	2.8	1.2	1
		2	N	43	1.1	4.6	6	1.7	1.9	4.2	6.1	2.3	2.3
	11	1	E	96	2.5	8.2	15.3	3	4.8	2	3.9	1.1	1.7
	12	1	E	104	2.7	9.9	15.5	3.7	4.8	2.4	3.2	1.3	1.2
	13	1	E	101	2.6	9.8	16.3	3.6	5.1	2	2.9	1.1	1.1
	14	1	E	93	2.4	10.4	15.4	3.9	4.8	1.8	2.5	1	1
	15	1	E	110	2.8	9.5	17.3	3.5	5.4	2.5	3	1.4	1.1
	16	1	E	100	2.6	8.5	11.7	3.1	3.7	2.5	3.7	1.4	1.4
		2	N	51	1.3	3.8	6.7	1.4	2.1	3	4.3	1.7	1.6
	17	1	E	101	2.6	12	13.5	4.4	4.2	2	3.7	1.1	1.4

E = enhancing tumor areas; N = nonenhancing tumor areas; Min = minimum; Max = maximum.

TABLE 4
HU on ceCT and 68Ga-PSMA and 18F-FDG Uptake from PET Data in Enhancing and Nonenhancing HCC Areas

Enhancement on ceCT	No. of areas	Mean HU	TBR-HU	68Ga-PSMA SUVmax	18F-FDG SUVmax	68Ga-PSMA TBR-SUVmax	18F-FDG TBR-SUVmax
Enhancing tumor areas	36	100.5 (91.3–114.8)	1.95 (1.5–2.5)	13.2 (9.5–15.4)	2.9 (2.6–3.5)	3.8 (2.5–4.7)	2.1 (1.6–2.8)
Nonenhancing tumor areas	10	48.5 (41.3–64.3)	0.85 (0.7–1.1)	6.2 (4.1–6.9)	5.9 (4.2–7.7)	1.6 (0.9–2.1)	1.2 (1–1.4)

Variables are expressed as medians, with 25%–75% interquartile ranges in parentheses.

and 4 regenerative nodules, were detected on CT and MRI. One patient had a solitary lesion, and 6 had multifocal or infiltrative disease. Table 2 summarizes the 68Ga-PSMA and 18F-FDG avidity of the tumor lesions and whether they were enhancing on CT or MRI.

Thirty-six of the 37 tumor lesions showed 68Ga-PSMA uptake higher than the background liver uptake. Twenty-eight of the tumor lesions showing increased 68Ga-PSMA uptake were non–18F-FDG–avid (Fig. 2), and 8 showed avidity for both tracers. All lesions showing 68Ga-PSMA avidity were associated with contrast enhancement on CT or MRI, representing hypervascularity—27 with homogeneous enhancement and 9 with a mosaic pattern composed of enhancing and nonenhancing areas (Fig. 3). The single HCC lesion that did not show increased 68Ga-PSMA uptake showed only mild peripheral contrast enhancement on CT and was primarily nonenhancing. It accumulated 18F-FDG. Several HCC lesions showed coexisting avidity for PET tracers and contrast enhancement (Fig. 4).

Table 3 summarizes the uptake values for the 2 PET tracers and the vascularity seen on CT in all lesions as well as in various areas within a lesion in the case of mosaic lesions. Vascularity was expressed as mean HU and TBR-HU on CT, and tracer uptake was expressed as SUVmin, SUVmax, and TBR-SUV for both 68Ga-PSMA and 18F-FDG.

Table 4 summarizes medians and interquartile ranges (25%–75%) for HU and uptake values for 68Ga-PSMA and 18F-FDG in enhancing and nonenhancing tumor areas. The Mann–Whitney test showed that 68Ga-PSMA uptake was significantly higher in enhancing tumor areas than in nonenhancing areas and, in contrast, that 18F-FDG uptake was higher in nonenhancing areas ($P < 0.001$ for both comparisons).

68Ga-PSMA uptake (68Ga-PSMA TBR-SUVmax) was found to correlate with vascularity (TBR-HU) (Spearman r, 0.866 [$P < 0.001$]; linear regression analysis: R^2, 0.752) (Fig. 5).

The 4 liver lesions identified as being hypodense on CT and negative on PET with either tracer were regenerative nodules, which remained unchanged on follow-up imaging. They showed uptake similar to that of the surrounding liver parenchyma.

To assess potential differential 68Ga-PSMA uptake in cirrhotic liver tissue, we compared 68Ga-PSMA uptake in the nontumor liver parenchyma in patients with cirrhosis ($n = 4$) and that in patients without cirrhosis ($n = 3$) and found no difference (68Ga-PSMA SUVmean, 3.3 [range, 2.5–3.8] and 3.9 [range, 3.2–4.4], respectively).

Two of the 7 patients (patients 1 and 7) had unexpected extrahepatic metastatic lesions on 68Ga-PSMA PET/CT. Patient 1 had increased uptake in a right adrenal mass. Treatment with liver radioembolization, which was the initial treatment plan, was altered to systemic treatment with sorafenib, a kinase inhibitor, and palliative radiotherapy to the right adrenal gland. Follow-up CT 2 mo later showed that the adrenal mass had increased in size. The patient died 7 mo later.

In patient 7 (Fig. 6), a peritoneal implant and bone marrow involvement were identified on 68Ga-PSMA PET/CT. The implant was seen on MRI as well. The patient died of advanced HCC 6 wk later.
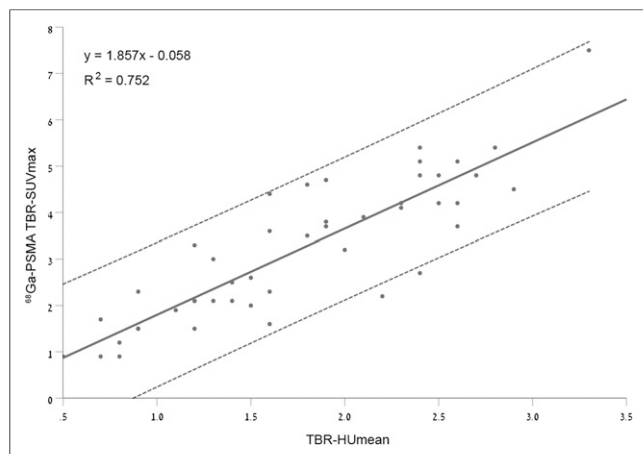
FIGURE 5. Linear regression and 95% CI correlating 68Ga-PSMA uptake and vascularity in HCC. max = maximum.
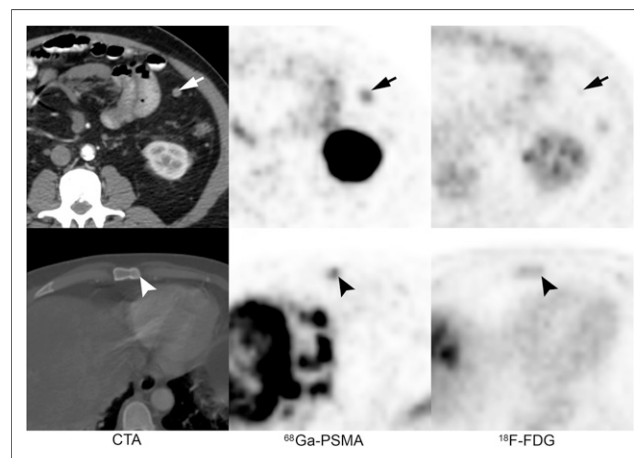
FIGURE 6. Unexpected bone metastasis in sternum (arrowheads) and implant in left upper quadrant (arrows) showing 68Ga-PSMA uptake and not 18F-FDG uptake. CTA = CT angiography.
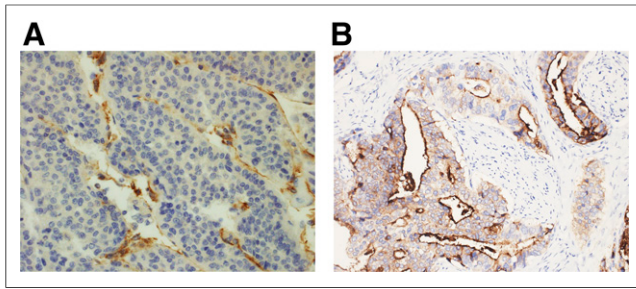
FIGURE 7. Immunohistochemical analysis of hypervascular HCC (A) and prostate cancer (B). (A) Intense intratumoral microvessel staining for PSMA (×40). (B) Positive staining for PSMA in cytoplasm and membrane, mainly in luminal border, but negative staining in blood vessels (×20).

Immunohistochemistry

In 3 of the 5 HCC samples analyzed, intense intratumoral microvessel staining for PSMA was noted. No staining was identified in epithelial tumor cells (Fig. 7A). The tumor biopsy sites showing intense PSMA staining were enhanced on CT (HU of 114, 99, and 140 and TBR-HU of 2, 1.6, and 1.6) and showed increased ^{68}Ga-PSMA uptake (Table 5), whereas the 2 negative areas were those obtained from nonenhancing lesions (HU of 53 and 67 and TBR-HU of 0.6 and 0.8). The latter 2 samples were obtained from patients who underwent only CT. In contrast, in the prostate cancer control, staining for PSMA was positive in the cytoplasm and membrane, mainly in the luminal border, but negative in the blood vessels (Fig. 7B).

DISCUSSION

^{68}Ga-PSMA is a PET tracer that was recently introduced for the PET/CT imaging of patients with prostate cancer. Its accumulation in prostate cancer tumor sites is the result of the overexpression of PSMA in tumor cells (7).

The incidental uptake of ^{68}Ga-PSMA has been described in other solid tumors, including case reports of HCC (9–11). In the present prospective pilot study, we investigated the uptake of ^{68}Ga-PSMA and of the routinely used ^{18}F-FDG in patients with HCC and compared it to contrast enhancement on CT or MRI for a total of 41 liver lesions detected in 7 patients. We also assessed by immunohistochemistry the location of PSMA staining in the tumoral tissue.

The imaging of liver lesions in cirrhotic patients is complex and challenging. The cirrhotic liver acquires a nodular architecture with altered vascularity, making difficult the differentiation of regenerative nodules from early HCC and metastases from other primary tumors. The challenge is even greater in patients who undergo ablative therapies for known HCC lesions. This complexity has resulted in the development of several staging algorithms, including RECIST, modified RECIST, and the Liver Reporting and Data System. Scores from these algorithms are frequently revised and are the focus of intense discussions (12–15).

Traditional imaging methods used in patients with HCC are ultrasound (with or without contrast) and multiphasic ceCT or MRI. Each method has its shortcomings, the major one being a lack of correlation between radiologic appearance and biologic activity.

PET/CT has so far not played a major role in the diagnosis or surveillance of HCC, and ^{18}F-FDG, the most commonly used tracer, is not routinely used in the initial workup of HCC. ^{18}F-FDG PET is taken up by metabolically active cells and, thus, tumor cells theoretically should show higher avidity for the isotope than normal cells. Despite this biologic reasoning, only a minority of HCCs take up ^{18}F-FDG (16). Our group recently reviewed data on ^{18}F-FDG PET/CT in HCC (6). The data suggested that ^{18}F-FDG PET/CT is a stronger predictor of prognosis and is superior to the assessment of tumor size or number of tumor nodules (as defined by the Milan criteria). These findings may have a direct impact on transplant outcome. ^{18}F-FDG PET/CT avidity in metabolically active tumors in patients for whom liver transplantation, resection, or ablation is planned may identify patients at risk for recurrence after each procedure (6). Furthermore, PET/CT may identify distant metastases that are difficult to discover using conventional imaging.

Although data on the use of PET/CT imaging in HCC are promising, this method is not recommended for routine use. The data are from small, retrospective reports, with variable criteria for interpreting PET/CT findings. Perhaps the most prominent problem is that ^{18}F-FDG is not taken up by all tumors, and there is suboptimal sensitivity ($<50\%$) of this modality for the detection of new HCCs, being inferior to CT (6). These findings were attributed to the fact that tumor metabolic activity was similar to that of adjacent liver tissue.

Because of the importance of functional PET imaging, a search for new tracers has been ongoing. A preliminary report showed that dual-tracer (^{11}C-acetate and ^{18}F-FDG) PET/CT was highly sensitive for the detection of HCC, reaching approximately 94%–95% sensitivity and 100% specificity, compared with much lower sensitivity rates for ceCT (detection rates of 67.6% and 37.5% for patients undergoing liver transplant and resection, respectively) (17).

TABLE 5
CT and PET Characteristics of HCC Biopsy Sites Showing Intense Intratumoral Microvessel Staining
for ^{68}Ga-PSMA on Immunohistochemical Analysis

Patient	Pathology	HU	TBR-HU	^{68}Ga-PSMA SUV$_{min}$	^{68}Ga-PSMA SUV$_{max}$	^{18}F-FDG SUV$_{min}$	^{18}F-FDG SUV$_{max}$
1	Well-differentiated HCC (G1)	114	2	9	11.7	1.4	1.8
3	Moderately differentiated HCC (G2)	99	1.6	10.5	17.5	3.8	6.5
6	Moderately differentiated HCC (G2)	140	1.6	25.6	41.2	1.8	2.7

Histologic grade of HCC = G1, well differentiated; G2, moderately differentiated.

The present pilot study showed encouraging preliminary results for ^{68}Ga-PSMA as a PET tracer for the imaging of HCC. All but a single tumor lesion were associated with tracer uptake higher than that of the surrounding liver parenchyma, with a mean uptake 3.6 times higher than that of the background liver. In contrast, only 10 of the malignant lesions were ^{18}F-FDG–avid. Increased ^{68}Ga-PSMA uptake identified unexpected metastatic lesions in bone marrow, an adrenal gland, and an abdominal implant. The explanation for the increased ^{68}Ga-PSMA uptake in HCC was provided by the results of immunohistochemistry analysis showing PSMA staining of the endothelial cell lining of vessels that are penetrated by a tumor. These findings are compatible with those of previous reports suggesting that nearly 95% of HCCs stain positive for PSMA in the tumor vasculature (18–20).

Conway et al. recently showed that PSMA plays a major role in regulating angiogenesis (21). The process was markedly reduced in mice deficient in PSMA. Its function was mediated via a regulatory loop that modulates laminin-specific integrin signaling and GTPase-dependent, p21-activated kinase 1 activity (21).

Zhu et al. suggested that the process of endothelial cell recruitment to HCC occurs early and throughout the process of hepatic tumorigenesis, making an endothelial cell tracer an ideal marker of early disease (22).

HCC is usually a highly vascular tumor characterized by early neoangiogenesis—the growth of functional collateral arteries covered with smooth muscle cells from preexisting arteries. HCC is mainly supplied by branches of the hepatic artery, whereas in the normal liver parenchyma, regenerative and dysplastic nodules are mainly supplied by the portal vein (23). Typically, in the arterial phase, there is minimal or no enhancement of the liver parenchyma and strong enhancement of hypervascular HCC lesions. During the delayed (portal) phase, there is rapid washout of contrast material from the tumor. These typical radiologic features have been incorporated into clinical practice guidelines (4), allowing for the diagnosis of HCC in cirrhotic patients without the need for biopsy. Enhancement on ceCT imaging was shown to correlate with microvessel density (23). Larger lesions are hypervascular unless rapid excessive tumor growth and further dedifferentiation occur; then, arterial flow may diminish, with larger areas of necrosis (24).

The results of the present study suggested a close correlation among intratumoral microvessel staining for PSMA, increased ^{68}Ga-PSMA uptake on PET, and lesion vascularity expressed on ceCT. Enhancing and nonenhancing lesions differed significantly in the uptake of PET tracers. Although enhancing lesions showed higher ^{68}Ga-PSMA uptake than nonenhancing lesions, the latter showed significantly higher uptake of ^{18}F-FDG. In mosaic lesions composed of islands of contrast enhancement, ^{68}Ga-PSMA also showed heterogeneity, with increased uptake corresponding to areas with high HU.

The present study has several limitations. The cohort was small—only 7 patients. However, 41 liver lesions were identified on CT and MRI and were available for assessment. In addition, the present study was an open study of patients with known HCC identified as HCC using conventional imaging before enrollment. Thus, the efficacy of ^{68}Ga-PSMA PET/CT that does not follow strict imaging criteria for HCC in diagnosing tumors or its role in reducing the need for biopsies is still questionable. Furthermore, the important distinction between early HCC and regenerative nodules needs to be validated.

In cirrhotic patients with a liver mass, current guidelines and clinical practice involve several imaging steps before biopsy is performed. PET imaging may be an early and cost-saving tool in this scenario.

CONCLUSION

Our findings suggest a potential role of ^{68}Ga-PSMA PET/CT in staging for patients with HCC and encourage the assessment of its role with a larger patient cohort.

DISCLOSURE

No potential conflict of interest relevant to this article was reported.

REFERENCES

1. Mittal S, El-Serag HB. Epidemiology of hepatocellular carcinoma: consider the population. *J Clin Gastroenterol.* 2013;47(suppl):S2–S6.
2. Zhu RX, Seto WK, Lai CL, et al. Epidemiology of hepatocellular carcinoma in the Asia-Pacific region. *Gut Liver.* 2016;10:332–339.
3. Lin CY, Chen JH, Liang JA, et al. ^{18}F-FDG PET or PET/CT for detecting extrahepatic metastases or recurrent hepatocellular carcinoma: a systematic review and meta-analysis. *Eur J Radiol.* 2012;81:2417–2422.
4. European Association for the Study of the Liver. EASL clinical practice guidelines: management of hepatocellular carcinoma. *J Hepatol.* 2018;69:182–236.
5. Agnello F, Salvaggio G, Cabibbo G, et al. Imaging appearance of treated hepatocellular carcinoma. *World J Hepatol.* 2013;5:417–424.
6. Asman Y, Evenson AR, Even-Sapir E, Shibolet O. [^{18}F]fludeoxyglucose positron emission tomography and computed tomography as a prognostic tool before liver transplantation, resection, and loco-ablative therapies for hepatocellular carcinoma. *Liver Transpl.* 2015;21:572–580.
7. Rauscher I, Maurer T, Fendler WP, Sommer WH, Schwaiger M, Eiber M. ^{68}Ga-PSMA ligand PET/CT in patients with prostate cancer: how we review and report. *Cancer Imaging.* 2016;16:14.
8. Patel D, Loh H, Le K, et al. Incidental detection of hepatocellular carcinoma on ^{68}Ga-labeled prostate-specific membrane antigen PET/CT. *Clin Nucl Med.* 2017;42:881–884.
9. Taneja S, Taneja R, Kashyap V, et al. ^{68}Ga-PSMA uptake in hepatocellular carcinoma. *Clin Nucl Med.* 2017;42:e69–e70.
10. Soydal C, Alkan A, Ozkan E, Demirkazık A, Kucuk NO. Ga-68 PSMA accumulation in hepatocellular carcinoma. *J Gastroenterol Pancreatol Liver Disord.* 2016;4:1–1.
11. Sasikumar A, Joy A, Nanabala R, et al. ^{68}Ga-PSMA PET/CT imaging in primary hepatocellular carcinoma. *Eur J Nucl Med Mol Imaging.* 2016;43:795–796.
12. Ramalho M, Matos AP, AlObaidy M, et al. Magnetic resonance imaging of the cirrhotic liver: diagnosis of hepatocellular carcinoma and evaluation of response to treatment—part 1. *Radiol Bras.* 2017;50:38–47.
13. Lyu N, Kong Y, Mu L, et al. Hepatic arterial infusion of oxaliplatin plus fluorouracil/leucovorin vs. sorafenib for advanced hepatocellular carcinoma. *J Hepatol.* 2018;69:60–69.
14. Choi MH, Park GE, Oh SN, et al. Reproducibility of mRECIST in measurement and response assessment for hepatocellular carcinoma treated by transarterial chemoembolization. *Acad Radiol.* March 16, 2018 [Epub ahead of print].
15. Kielar AZ, Chernyak V, Bashir MR, et al. LI-RADS 2017: an update. *J Magn Reson Imaging.* 2018;47:1459–1474.
16. Li YC, Yang CS, Zhou WL, et al. Low glucose metabolism in hepatocellular carcinoma with GPC3 expression. *World J Gastroenterol.* 2018;24:494–503.
17. Larsson P, Arvidson D, Björnstedt M. et al. Adding ^{11}C-acetate to ^{18}F-FDG at PET examination has an incremental value in the diagnosis of hepatocellular carcinoma. *Mol Imaging Radionucl Ther.* 2012;21:6–12.
18. Liu H, Moy P, Kim S, et al. Monoclonal antibodies to the extracellular domain of prostate-specific membrane antigen also react with tumor vascular endothelium. *Cancer Res.* 1997;57:3629–3634.
19. Chen Y, Dhara S, Banerjee SR, et al. A low molecular weight PSMA-based fluorescent imaging agent for cancer. *Biochem Biophys Res Commun.* 2009;390:624–629.
20. Mhawech-Fauceglia P, Zhang S, Terracciano L, et al. Prostate-specific membrane antigen (PSMA) protein expression in normal and neoplastic tissues and its sensitivity and specificity in prostate adenocarcinoma: an immunohistochemical study using multiple tumour tissue microarray technique. *Histopathology.* 2007;50:472–483.
21. Conway RE, Petrovic N, Li Z, et al. Prostate-specific membrane antigen regulates angiogenesis by modulating integrin signal transduction. *Mol Cell Biol.* 2006;26:5310–5324.
22. Zhu H, Shao Q, Sun X, et al. The mobilization, recruitment and contribution of bone marrow-derived endothelial progenitor cells to the tumor neovascularization occur at an early stage and throughout the entire process of hepatocellular carcinoma growth. *Oncol Rep.* 2012;28:1217–1224.
23. Muto J, Shirabe K, Sugimachi K, et al. Review of angiogenesis in hepatocellular carcinoma. *Hepatol Res.* 2015;45:1–9.
24. Choi JY, Lee JM, Sirlin CB. CT and MR imaging diagnosis and staging of hepatocellular carcinoma: part I. Development, growth, and spread: key pathologic and imaging aspects. *Radiology.* 2014;272:635–654.